2024 IEEE 63rd Conference on Decision and Control (CDC)
December 16-19, 2024. MiCo, Milan, Italy

Nonlinear Observers with Tighter Online Error Bounds

João Pedro Silvestre[1], Rahal Nanayakkara[1], and Paulo Tabuada[1]

2024 IEEE 63rd Conference on Decision and Control (CDC) | 979-8-3503-1633-9/24/$31.00 ©2024 IEEE | DOI: 10.1109/CDC56724.2024.10885855

***Abstract*— Estimation algorithms and nonlinear observers are widespread tools used in a variety of real-world applications, from satellite control to epidemiological studies. Their primary purpose is to provide an estimate of the state computed from available measurements and a model of the dynamics. When state estimates are used to enforce safety properties, it is essential to understand and characterize how accurate these estimates are so that safety is still guaranteed. While several observer design techniques provide bounds for the estimation error, they are either computationally expensive or too conservative and thus difficult to use in practice. Our work tackles these issues by providing error bounds for observers based on Savitzky-Golay filtering which are applicable to nonlinear systems satisfying a suitable observability assumption. Moreover, the error bounds are computed online based on measured data are thus tighter than offline bounds based on worst case assumptions.**

We generalize prior theoretical results by some of the authors from polynomial approximations to other functions and use this added flexibility to obtain tighter bounds. Finally, we illustrate the results using multiple examples, including an application to in-host models used in epidemiology.

I. Introduction

The recent interest in safety as a control design objective [1] has brought a new focus on observers since safety enforcing techniques, such as control barrier functions [2], [3], rely on state estimates. It is, therefore, critical to provide formal guarantees on the error of such estimates. Unfortunately, all the observer design techniques providing error bounds, known by the authors, either yield worst-case offline bounds or require highly structured systems with a significant computational footprint.

Notably, only a handful of estimation algorithms explicitly provide deterministic bounds on the error, with set-valued observers being one of the few examples [4]. However, their applications are often limited due to requiring linear or highly structured control systems [5]. Similarly, interval observers [6] are commonly utilized for providing time-varying bounds, yet they suffer from similar system restrictions as set-valued observers. Although there are observer design techniques providing offline error bounds [7], they tend to be too conservative due to the worst-case nature of their formulation/computation.

Other strategies that focus on different guarantees offer asymptotic or ISS properties in the presence of noise [8]. In the context of safety, asymptotic properties tend to be less useful since safety is to be enforced at each time instant and not just asymptotically. Moreover, ISS bounds tend to be too conservative, given they are typically obtained indirectly, *e.g.*, via Lyapunov functions.

Many control barrier function frameworks use ISS observers to ensure the safety of the closed-loop system [9]. Other works use disturbance observers [10] to derive controllers capable of dealing with disturbances or use robust Lyapunov functions [11] to cope with measurement errors. All of these techniques, however, rely on worst-case offline characterizations of the estimation error. As these bounds tend to be very conservative, the guarantees of these methods became less useful.

In contrast with the previously described results, online bounds offer the promise of reducing conservatism since they can adapt to the evolution of the system and the available measurements. Recently, some of the authors introduced a new technique to compute online error bounds for observers designed via Savitzky-Golay filtering [12]. In this paper, we extend the scope of the previous work and improve its performance while maintaining a minimal computational footprint. We numerically validate our theoretical results in several examples, including an in-host model describing the evolution of COVID in infected patients. In particular, this example illustrates how the choice of sampling rate is essential since error bounds can be substantially tightened by increasing the measurement frequency.

The main contributions of this paper are thus threefold:

1) We generalize the results in [12] by using arbitrary smooth functions to approximate the data rather than polynomials.
2) We further extend the theoretical analysis in [12] by decoupling the estimator choice from the error bounds, thereby providing tighter error bounds on the state estimates.
3) We show how the error bounds are practically useful for monitoring the evolution of COVID infections in patients.

II. Problem Setup

We start by considering a nonlinear control system given by:

$$\begin{aligned} \dot{x} &= f(x,u) \\ y &= h(x,u), \end{aligned} \tag{1}$$

where $x \in \mathbb{R}^n$ represents the state of system, $u \in \mathbb{R}^m$ the control input, $y \in \mathbb{R}^p$ the output, and both $f : \mathbb{R}^n \times \mathbb{R}^m \to \mathbb{R}^n$ and $h : \mathbb{R}^n \times \mathbb{R}^m \to \mathbb{R}^p$ are sufficiently

The work of João Pedro Silvestre was supported by the PhD Grant 2023.01843.BD from the Fundação para a Ciência e a Tecnologia (FCT), Portugal. Additionally, this work was partially supported by NSF awards 2211146 and 2146828.

[1]João Pedro Silvestre, Rahal Nanayakkara, and Paulo Tabuada are with the Electrical and Computer Engineering Department, University of California at Los Angeles, Los Angeles, CA 90095 USA (e-mail: {joaosilvestre, tabuada}@ucla.edu).

regular maps to ensure existence and uniqueness of solutions. Our objective is to estimate the state $x(t)$ given $N+1$ noise corrupted measurements $\{y_{m0}, ..., y_{mN}\}$, at discrete time instants $\{t_0, ..., t_N\}$, where $y_m(t) = y(t) + w(t)$, and w represents measurement noise. Denoting by $y^{(d)} \in \mathbb{R}^p$ the derivative of order d of y with respect to time and $u^{(d)} \in \mathbb{R}^m$ as the derivative of order d of u with respect to time, our approach is based on the following notion of observability.

Assumption 1. The control system (1) is differentially observable of order d. In particular, there exists a continuous function $\mathcal{L}$ that maps the d derivatives of the output $y(t)$ and input $u(t)$ to the state $x(t)$, *i.e.*:

$$(y(t), \dot{y}(t), ..., y^{(d)}(t), u(t), u(t), ..., u^{(d)}(t)) \xmapsto{\mathcal{L}} x(t). \quad (2)$$

Under mild assumptions, see [13, Chapter 4], differential observability is known to be a generic property and thus a good starting point for out theoretical developments. Furthermore, under assumption 1, the problem of estimating the state is reduced to the problem of estimating the derivatives of the output. Hence, the problem addressed in this paper is: how to estimate the derivatives of the output so as to provide an online error bound on the resulting state estimate?

III. Estimating derivatives and computing error bounds

A. Computing Derivatives

From the differential observability assumption, it is clear that as long as we can estimate the first d derivatives of the output, it is possible to estimate the state of the nonlinear system. Thus, in this section, we focus on computing the derivatives of the output.

Let us start by assuming the output, y, to be $d+1$ times continuously differentiable and one dimensional, as the extension to the multidimensional case is straightforward. Using the measurements of y at the instants $\{t_0, t_1, \ldots, t_N\}$ we construct a function $g : \mathbb{R} \to \mathbb{R}$ approximating y on the interval $[t_0, t_N]$. Our results are agnostic to how g is computed as long as it is $d+1$ times continuously differentiable. In practice, g is described by a finite number of parameters (e.g., a polynomial), and we find the parameters that lead to the best fit of $g(t_i)$ to $y(t_i)$ for all $i \in \{t_0, t_1, \ldots, t_N\}$.

Lastly, we exploit the fact that g approximates y, and, similarly to Savitzky-Golay filtering [13], approximate the first d derivatives of y by differentiating the smooth function g.

B. Computing the Derivatives' Error

Although g may approximate well y at the discrete time instants, there is no guarantee that it may also do so at every point in $[t_0, t_N]$. To estimate the worst-case fit between g and y, we use the idea of residual interpolant commonly used in functional approximation. In this case, we use a degree-d polynomial defined by:

$$r(s_i) := y(s_i) - g(s_i), \quad \forall s_i \in \mathcal{D}, \quad (3)$$

where $\mathcal{D} := \{s_0, ..., s_d\} \subseteq \{t_0, ..., t_N\}$, and $d > 0$. Note that r is uniquely determined since it is a polynomial of degree d interpolating d+1 points.

Our first and foremost result uses the residual polynomial to compute an exact equality for the estimation error $e^{(k)} := y^{(k)} - g^{(k)}$, where $k \in \mathbb{N}$. Beforehand, we define $v_i \in \mathbb{R}_{\geq 0}$ as the time instant where the i-th zero of $e^{(k)} - r^{(k)}$ occurs.

Theorem 1. For any $t \in [s_0, s_d]$, the following equality holds:

$$e^{(k)}(t) = r^{(k)}(t) + \frac{e^{(d+1)}(\xi_t)}{(d-k+1)!} \prod_{i=0}^{d-k} (t - v_i), \quad (4)$$

where $\xi_t \in [s_0, s_d]$ is a function of t.

Proof. Let us start by defining the function $q : \mathbb{R} \to \mathbb{R}$ as:

$$q(t) := e(t) - r(t). \quad (5)$$

It follows by construction that $q(t) = 0, \ \forall t \in \mathcal{D}$. Since $\mathcal{D}$ has $d+1$ elements, q has at least $d+1$ zeros. Hence, by Rolle's Theorem, $q^{(k)}$ has at least $d-k+1$ zeros, and thus, we define $\mathcal{V} := \{v_0, ..., v_{d-k}\}$ as the set containing $d-k+1$ zeros of $q^{(k)}$.

We now define a family of functions $h_t : \mathbb{R} \to \mathbb{R}$ parameterized by $t \in [s_0, s_d]$:

$$h_t(z) = q^{(k)}(z) - \alpha_t \prod_{i=0}^{d-k} (z - v_i), \quad (6)$$

for some $\alpha_t \in \mathbb{R}$. The parameter α_t, a function of t, is defined so that the equality $h_t(t) = 0$ holds for every t. Such choice of α_t exists since for $t = v_i$, both $q^{(k)}(t)$ and $\prod_{i=0}^{d-k}(t - v_i)$ are zero and the choice of α_t is inconsequential. When $t \neq v_i$, then α_t exists since $\prod_{i=0}^{d-k}(t - v_i)$ is non-zero. When α_t ensures $h_t(t) = 0$, we assert that $h_t(z)$ has $d-k+2$ zeros, namely $z = v_i$ and $z = t$. Hence, using Rolle's Theorem there exists some $\xi_t \in \mathbb{R}$ such that $h^{(d-k+1)}(\xi_t) = 0$. Thus, we compute α_t as:

$$\begin{aligned} 0 = h_t^{(d-k+1)}(\xi_t) &= q^{(d+1)}(\xi_t) - \alpha_t (d-k+1)! \\ &= e^{(d+1)}(\xi_t) - \alpha_t (d-k+1)! \\ \Rightarrow \alpha_t &= \frac{e^{(d+1)}(\xi_t)}{(d-k+1)!}. \end{aligned} \quad (7)$$

Finally, using (6), for any $t \in [s_0, s_d]$ the error $e^{(k)}(t)$ is given by:

$$e^{(k)}(t) = r^{(k)}(t) + \frac{e^{(d+1)}(\xi_t)}{(d-k+1)!} \prod_{i=0}^{d-k} (t - v_i). \quad (8)$$

■

This approach provides an exact formula for the error at any $t \in [s_0, s_d]$, however, in practice, we do not know where the zero of $h^{(d-k+1)}$ occurs, and therefore we cannot find ξ_t. Thus, our next step is to use Theorem 1 to design an online bound that can be computed using the available information, *i.e.*, known bounds on y and g, the model of the control system, and the available measurements.

C. Computing Error Bounds

We transform equality (8) into a bound that can be computed online by first considering the case where $k = 0$ and then extending such bound for $0 < k \leq d$.

Beforehand, we note that providing error bounds for the estimates of output derivatives without any assumptions on the differentiated signal is impossible. Thus, we make general assumptions on this signal, such as the knowledge of a bound on one of its derivatives.

Assumption 2. There exist constants $Y_d, G_d, W \in \mathbb{R}_0^+$ such that for every $\xi_t \in [s_0, s_d]$ the following inequalities hold: $Y_d \geq |y(\xi_t)^{(d+1)}|$ and $G_d \geq |g(\xi_t)^{(d+1)}|$, and for all $t \in [s_0, s_d]$, $W \geq |w(t)|$.

In practice, it is easier to compute a tighter upper bound G_d than Y_d since we can choose the function g. Now, the first result we derive is a bound on the estimation error between the measured output $y_m := y + w$ and the smooth estimation model g. Beforehand, let us denote the Lagrange basis polynomials for $\mathcal{D}$ as $l_i : \mathbb{R} \to \mathbb{R}$ with $i = 0, 1, ..., d$, defined as:

$$l_i(t) = \prod_{s_j \in D \setminus s_i} \frac{t - s_j}{s_i - s_j}. \tag{9}$$

This polynomial basis ensures the residual follows (3), allowing us to separate two different components, the error of the noisy measurements $e(t) + w(t)$, and the noise signal $w(t)$.

Corollary 1. Let $d > 0$, and assume the existence of an upper bound $\sigma > 0$ for the maximum inter-sample time, i.e., $s_{i+1} - s_i \leq \sigma$ for all $i \in \{0, 1, \ldots, d-1\}$. The following inequality holds:

$$\begin{aligned} |e(t)| \leq & \Big| \sum_{s_i \in D} l_i(t)(e(s_i) + w(s_i)) \Big| \\ & + \sum_{s_i \in D} \Big| l_i(t) \Big| W + \frac{(Y_d + G_d)\sigma^{d+1}}{4(d+1)}. \end{aligned} \tag{10}$$

Proof. We bound the estimation error by:

$$\begin{aligned} e(t) &= e(t) + w(t) - w(t) \\ &\leq |e(t) + w(t)| + W, \end{aligned} \tag{11}$$

and bound the residual as follows:

$$\begin{aligned} r(t) &= \sum_{s_i \in D} l_i(t) e(s_i) \\ &\leq \Big| \sum_{s_i \in D} l_i(t) e(s_i) \Big| \\ &\leq \Big| \sum_{s_i \in D} l_i(t)(e(s_i) + w(s_i)) \Big| + \Big| \sum_{s_i \in D} l_i(t) w(s_i) \Big| \\ &\leq \Big| \sum_{s_i \in D} l_i(t)(e(s_i) + w(s_i)) \Big| + \sum_{s_i \in D} \Big| l_i(t) \Big| W. \end{aligned} \tag{12}$$

Then, we use (12) and (8) to bound $|e(t)|$ by:

$$\begin{aligned} |e(t)| \leq & \Big| \sum_{s_i \in D} l_i(t)(e(s_i) + w(s_i)) \Big| + \sum_{s_i \in D} \Big| l_i(t) \Big| W \\ & + \frac{Y_d + G_d}{(d+1)!} \prod_{i=0}^{d} |t - v_i|. \end{aligned} \tag{13}$$

Now, we consider the worst-case scenario, when t is exactly at the center of either $[s_0, s_1]$ or $[s_{d-1}, s_d]$. In that case, there are exactly $d + 1$ zeros and their distance to t ranges from $1/2\sigma$ up to $d\sigma$. We note that the first two zeros both have a distance of $1/2\sigma$, since t is in the middle of two samples. Therefore, we use the bound:

$$\begin{aligned} \frac{Y_d + G_d}{(d+1)!} \prod_{i=0}^{d} |t - v_i| &\leq \frac{(Y_d + G_d)\sigma}{4(d+1)!} \prod_{i=1}^{d} i\sigma \\ &\leq \frac{(Y_d + G_d)\sigma^{d+1}}{4(d+1)}. \end{aligned} \tag{14}$$

Finally, we substitute (14) into (13) to compute the overall bound as:

$$\begin{aligned} |e(t)| \leq & \Big| \sum_{s_i \in D} l_i(t)(e(s_i) + w(s_i)) \Big| \\ & + \sum_{s_i \in D} \Big| l_i(t) \Big| W + \frac{(Y_d + G_d)\sigma^{d+1}}{4(d+1)}. \end{aligned} \tag{15}$$

■

The strategy in the proof of Corollary 1 can also be exploited to obtain a bound when $k > 0$.

Corollary 2. Let $d > 0$, $d \geq k > 0$, and assume the existence of an upper bound $\sigma > 0$ for the maximum inter-sample time, i.e., $s_{i+1} - s_i \leq \sigma$ for all $i \in \{0, 1, \ldots, d-1\}$. The following inequality holds:

$$\begin{aligned} |e^{(k)}(t)| \leq & \Big| \sum_{s_i \in D} l_i^{(k)}(t)(e(s_i) + w(s_i)) \Big| \\ & + \sum_{s_i \in D} \Big| l_i^{(k)}(t) \Big| W + (Y_d + G_d)\sigma^{d-k+1} \binom{d}{k-1}. \end{aligned} \tag{16}$$

Proof. Let us begin by reconsidering the bound (13), and the worst possible scenario, when t is equal to s_0 or s_d. In that case, we know there are $d - k + 1$ zeros, each with a maximum distance to t ranging from $k\sigma$ to $d\sigma$. Therefore, we use the bound.

$$\begin{aligned} \frac{1}{(d-k+1)!} \prod_{i=0}^{d-k} |t - v_i| &\leq \frac{1}{(d-k+1)!} \prod_{i=k}^{d} i\sigma \\ &\leq \frac{\sigma^{d-k+1} d!}{(d-k+1)!(k-1)!}. \\ &\leq \sigma^{d-k+1} \binom{d}{k-1}. \end{aligned} \tag{17}$$

Finally, the overall bound is given by:

$$|e^{(k)}(t)| \leq \Big| \sum_{s_i \in D} l_i^{(k)}(t)(e(s_i) + w(s_i)) \Big| + \sum_{s_i \in D} \Big| l_i^{(k)}(t) \Big| W + (Y_d + G_d)\sigma^{d-k+1} \binom{d}{k-1}. \tag{18}$$

■

D. Gaussian Estimator

In this section, we exploit the flexibility afforded by the ability to choose the function g. In prior work [12] g was assumed to be a polynomial. Instead, we consider a sum of Gaussians and show in section IV how this choice leads to tighter error bounds.

The Gaussian estimator is constructed from $N+1$ measurements using $n < N+1$ Gaussian functions:

$$\gamma_i(t) = e^{\frac{-(t-t_i)^2}{2c^2}}, \tag{19}$$

where $t_i \in [t_0, t_N]$ represents the center of γ_i and $c \in \mathbb{R}_{>0}$ is the standard deviation. The function $g(t)$ is then defined as:

$$g(t) = \sum_{i=0}^{n-1} \theta_i \gamma_i(t), \tag{20}$$

where $\theta = [\theta_0, \ldots, \theta_{n-1}] \in \mathbb{R}^n$ is a constant parameter to be chosen so as to maximize the fit between $y(t_i)$ and $g(t_i)$. To compute θ, we consider $\gamma = [\gamma_0, \ldots, \gamma_{n-1}]$, and solve the least-squares problem formulated as:

$$\theta = \arg\min_{\theta} \sum_{i=0}^{N} ||y_m(t_i) - \gamma(t_i)\theta||_2^2. \tag{21}$$

The function (20) can approximate arbitrarily well n points given n Gaussian functions and an appropriate c. In practice, however, we found it preferable to use a smaller number of Gaussians to reduce the impact of measurement noise. The reason for using Gaussian functions comes from the larger number of parameters to tune, which empirically leads us to conclude that these functions are able to provide better bounds.

IV. Simulation Results

In this section, we show, via numerical simulations, how the proposed results improve upon the polynomial observer in [12]. We also consider the concrete example of estimating the internal states of patients infected with COVID when using an in-host model describing the evolution of the infection.

A. Improvement in error bounds

Consider the first example presented in [12], *i.e.*, the Lorenz attractor system, defined by:

$$\begin{aligned} \dot{x_1} &= s(x_2 - x_1) \\ \dot{x_2} &= x_1(\rho - x_3) - x_2, \qquad y = x_1, \\ \dot{x_3} &= x_1 x_2 - \beta x_1 \end{aligned} \tag{22}$$

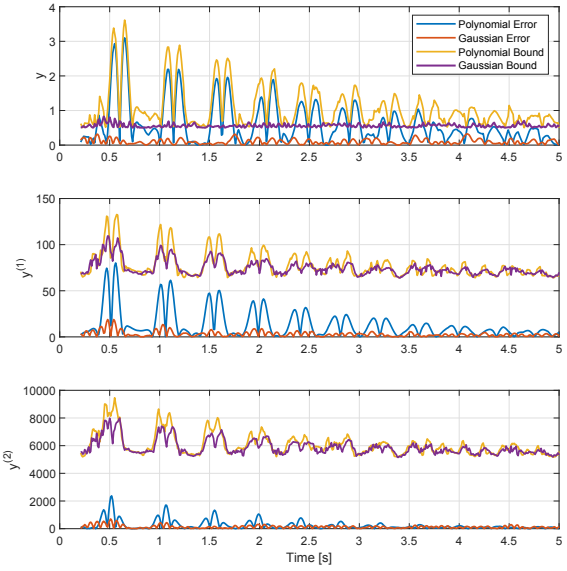

Fig. 1. Comparison of the error and bound of the first two derivatives of the Lorentz system between the degree-2 polynomial and the Gaussian estimator.

where $s = 7$, $\rho = 45$ and $\beta = 5.5$. The output estimation is based on a sampling window with 21 samples and a 100Hz sampling rate. The Gaussian estimator used 5 Gaussian functions, each with a standard deviation of $c = 0.15$. To display the power both observers have to cope with measurement noise, a white noise signal was added to the output y, with a standard deviation of 0.15 and $W = 0.5$. The result in Fig. 1 used a degree-2 polynomial observer, while the results in Fig. 2 and Fig. 3 used a degree-3 polynomial observer.

Firstly, as depicted in Fig. 1, it is evident that the Gaussian estimator exhibits a much lower estimation error compared to the polynomial while having a similar error bound, with an equal floor but a lower peak. The main factor contributing to the high estimation error in the case of the degree-2 polynomial function is the choice of the order of the observer. To prevent a larger estimation bound on the derivatives, we opted for a lower-order polynomial than the one required by the Lorenz system. Consequently, the estimation function was not well-suited for the highly nonlinear output, leading to an estimation error that reached a peak of 3 in the output and 75 in the derivative.

The output estimation presented in Fig. 2 depicts the estimation results with a degree-3 polynomial. While this approach led to a significant reduction in estimation error, it also resulted in an increase in the error bound. The reason behind not using a larger degree polynomial lies in the limitation of the previous work [12], which could not increase the degree of the polynomial, without loosening the bounds. In contrast, the Gaussian estimator displayed a superior bound and yielded better estimation results. This comparison shows how decoupling the estimation function or

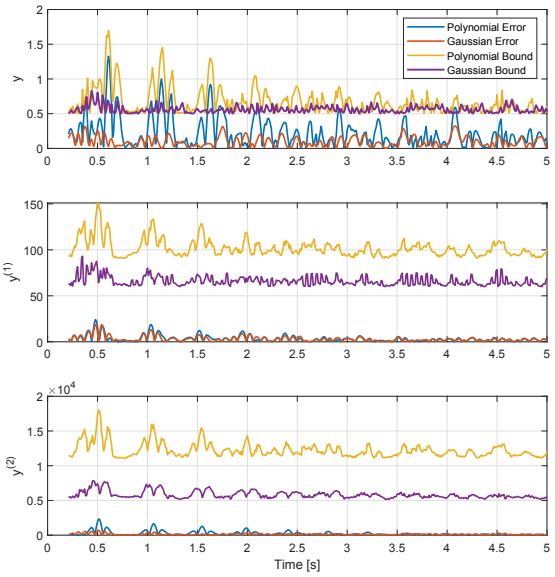

Fig. 2. State estimation error and bounds of the Lorentz system between the degree-3 polynomial and the Gaussian estimator.

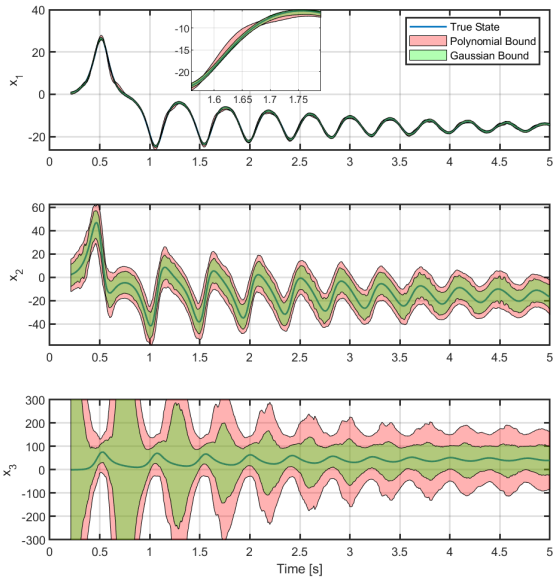

Fig. 3. State Bounds for the polynomial and the Gaussian estimators. Each bound is shaded differently, and the darker green indicates the area where the bounds overlap.

model from the polynomial order of the residual allows for a more effective estimation function without compromising the error bound.

Finally, Fig. 3 displays how the state estimation bound was influenced by the change in output bound shown in Fig. 2. While the third state has a bound which does not provide much information, this is caused by the estimation of x_3 requiring the second derivative of x_1. We conclude from this result that our work enables tighter bounds, allowing a better state estimation result without compromise.

B. Applications to Epidemiology

We now present the application to an epidemiological model, specifically the Target Cell Limited (TCL) model for acute infections [14], [15], where the in-host dynamics are described by the following set of differential equations:

$$\begin{aligned} \dot{U}(t) &= -\beta U(t)V(t) \\ \dot{I}(t) &= \beta U(t)V(t) - \delta I(t) \\ \dot{V}(t) &= pI(t) - cV(t). \end{aligned} \tag{23}$$

Here, U [cells] denotes the number of uninfected/susceptible cells; I [cells] denotes the number of infected cells; and V [copies.mL^{-1}] represents the concentration of viral particles The model parameters β [mL.copies^{-1}.day^{-1}] represents the infection rate of healthy cells, δ [day^{-1}] represents the death rate of infected cells, p [copies.mL^{-1}.cells^{-1}.day^{-1}] represents the viral replication rate, and c [day^{-1}] represents the clearance rate of the virus. The observable output, $y(t)$, of this model will be the viral load, $V(t)$, which can be measured at discrete time instances using testing methods such as ddPCR [16]. We also note that this model satisfies the property of being differentially observable, with the mapping between the output and internal states being given by:

$$\begin{aligned} V &= y \\ I &= \frac{1}{p}(\dot{y} + cy) \\ U &= \frac{1}{p\beta y}(\ddot{y} + (\delta + c)\dot{y} + \delta c y). \end{aligned} \tag{24}$$

It is important to note that the state U is only observable for non-zero viral load, as the mapping is only well defined when $y \neq 0$.

In our simulations, we look at the scenario where an infected patient is being closely monitored in urgent care, with viral load measurements being taken at intervals of 6 hours. In such a situation it is critical to accurately estimate the amount of uninfected and infected cells within the patient, to assess the patient's condition and make informed decisions regarding the patient's treatment and care plan.

Fig. 4 shows the evolution of the internal states of such a host, undergoing a viral infection. The model parameters used were $\beta = 1\times10^{-8}$, $\delta = 1.07$, $p = 2$ and $c = 2.3$. These values were sampled from the parameter ranges determined for modeling the infection process of COVID-19, based on collected data [15]. The graphical results show the effectiveness of the proposed observer in accurately estimating all the internal states throughout the entire infection period, as well as producing precise estimation error bounds for I and V. However, we note that the error bound for the estimate of U diverges when the viral load is extremely low, as the output to state map approaches a singularity. But, this divergence occurs either during the early stages of infection or when the

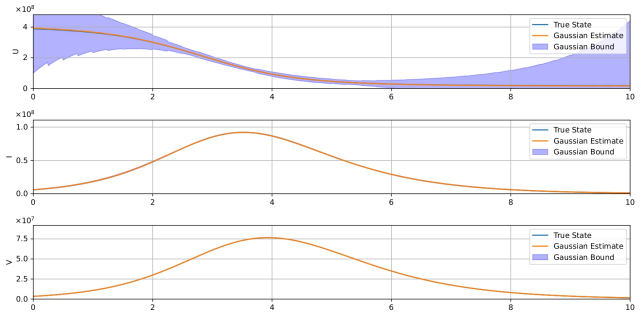

Fig. 4. Estimation of states in the TCL viral dynamics model using Gaussian estimators, with $N = 6$ and $n = 5$

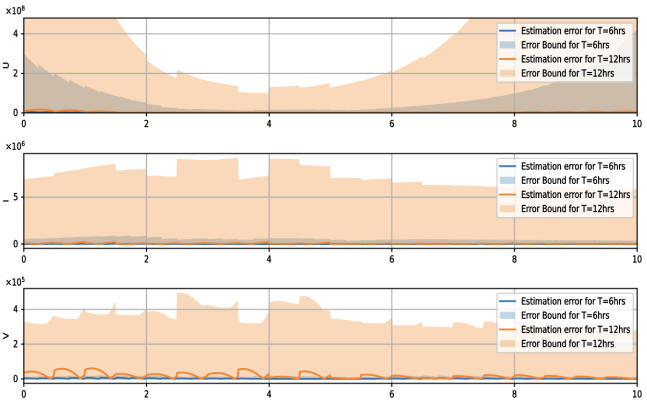

Fig. 5. Comparison of estimation error and error bound for states in the TCL viral dynamics model using Gaussian estimators, with $N = 6$ and $n = 5$, for sampling times of 6 hours and 12 hours

host is nearing recovery, both of which are comparatively less severe situations. In contrast, during the more critical phase of the infection, characterized by a high level of infected cells and viral load, the observer bound for U converges to a significantly smaller range, providing a more confident estimate.

Fig. 5 compares the estimation error and the associated bound obtained for the same patient being tested at two different sampling frequencies; once every 6 hours and once every 12 hours. This highlights the importance of using a sufficiently high sampling rate to obtain a precise bound on the estimation error, as it can be observed that decreasing the sampling time by a factor of 2 has reduced the error bound by more than an order of magnitude.

Our algorithm provides tight bounds on the estimation error provided the sampling rate can be chosen sufficiently high, as depicted in the studied case, where a sampling period of 6 hours was used. As testing becomes cheaper, this provides an excellent opportunity to closely monitor the evolution of the infection in the hospitalized population.

V. Conclusion

In this paper, we introduce a Savitzky-Golay observer with improved error bounds. Our contribution improves on previous work by allowing for non-polynomial approximating functions which, in turn, lead to tighter error bounds by working with, e.g., sums of Gaussian functions. The algorithm has been compared with prior work, showing notable enhancements in performance.

Furthermore, we applied the algorithm to address an epidemiological problem, displaying its practical utility in real-world scenarios. Several questions remain open for future research such as the choice of approximating functions and the optimal choice of the set $\mathcal{D}$.

References

[1] F. Ferraguti, C. T. Landi, A. Singletary, H.-C. Lin, A. Ames, C. Secchi, and M. Bonfè, "Safety and efficiency in robotics: the control barrier functions approach," *IEEE Robotics & Automation Magazine*, vol. 29, no. 3, pp. 139–151, 2022.

[2] X. Xu, P. Tabuada, J. W. Grizzle, and A. D. Ames, "Robustness of control barrier functions for safety critical control," *IFAC-PapersOnLine*, vol. 48, no. 27, pp. 54–61, 2015.

[3] A. D. Ames, X. Xu, J. W. Grizzle, and P. Tabuada, "Control barrier function based quadratic programs for safety critical systems," *IEEE Transactions on Automatic Control*, vol. 62, no. 8, pp. 3861–3876, 2016.

[4] P. Rosa, C. Silvestre, J. S. Shamma, and M. Athans, "Fault detection and isolation of LTV systems using set-valued observers," in *49th IEEE Conference on Decision and Control (CDC)*. IEEE, 2010, pp. 768–773.

[5] J. S. Shamma and K.-Y. Tu, "Set-valued observers and optimal disturbance rejection," *IEEE Transactions on Automatic Control*, vol. 44, no. 2, pp. 253–264, 1999.

[6] A. Khan, W. Xie, B. Zhang, and L.-W. Liu, "A survey of interval observers design methods and implementation for uncertain systems," *Journal of the Franklin Institute*, vol. 358, no. 6, pp. 3077–3126, 2021.

[7] S. Diop, "Observers for sampled data nonlinear systems via numerical differentiation," in *2007 European Control Conference (ECC)*. IEEE, 2007, pp. 1179–1184.

[8] A. Alessandri, "Observer design for nonlinear systems by using input-to-state stability," in *2004 43rd IEEE Conference on Decision and Control (CDC)(IEEE Cat. No. 04CH37601)*, vol. 4. IEEE, 2004, pp. 3892–3897.

[9] S. Kolathaya and A. D. Ames, "Input-to-state safety with control barrier functions," *IEEE control systems letters*, vol. 3, no. 1, pp. 108–113, 2018.

[10] A. Alan, T. G. Molnar, E. Daş, A. D. Ames, and G. Orosz, "Disturbance observers for robust safety-critical control with control barrier functions," *IEEE Control Systems Letters*, vol. 7, pp. 1123–1128, 2022.

[11] K. Garg and D. Panagou, "Robust control barrier and control Lyapunov functions with fixed-time convergence guarantees," in *2021 American Control Conference (ACC)*. IEEE, 2021, pp. 2292–2297.

[12] J. Bunton and P. Tabuada, "Confidently incorrect: nonlinear observers with online error bounds," *2024 American Control Conference (ACC)*, 2024, to appear.

[13] A. Savitzky and M. J. Golay, "Smoothing and differentiation of data by simplified least squares procedures." *Analytical chemistry*, vol. 36, no. 8, pp. 1627–1639, 1964.

[14] S. M. Ciupe and J. M. Heffernan, "In-host modeling," *Infectious Disease Modelling*, vol. 2, no. 2, pp. 188–202, 2017.

[15] E. A. Hernandez-Vargas and J. X. Velasco-Hernandez, "In-host mathematical modelling of COVID-19 in humans," *Annual reviews in control*, vol. 50, pp. 448–456, 2020.

[16] T. Suo, X. Liu, J. Feng, M. Guo, W. Hu, D. Guo, H. Ullah, Y. Yang, Q. Zhang, X. Wang *et al.*, "ddPCR: a more accurate tool for sars-cov-2 detection in low viral load specimens," *Emerging microbes & infections*, vol. 9, no. 1, pp. 1259–1268, 2020.